JACS
JOURNAL OF THE AMERICAN CHEMICAL SOCIETY
Communication
pubs.acs.org/JACS

Tunable Mid-Infrared Localized Surface Plasmon Resonances in Silicon Nanowires

Li-Wei Chou, Naechul Shin, Saujan V. Sivaram, and Michael A. Filler*

School of Chemical & Biomolecular Engineering, Georgia Institute of Technology, Atlanta, Georgia 30332, United States

Supporting Information

ABSTRACT: We observe and systematically tune an intense mid-infrared absorption mode that results from phosphorus doping in silicon nanowires synthesized via the vapor−liquid−solid technique. The angle- and shape-dependence of this spectral feature, as determined via *in-situ* transmission infrared spectroscopy, supports its assignment as a longitudinal localized surface plasmon resonance (LSPR). Modulation of resonant frequency (740−1620 cm^{-1}) is accomplished by varying nanowire length (135−1160 nm). The observed frequency shift is consistent with Mie−Gans theory, which indicates electrically active dopant concentrations between 10^{19} and 10^{20} cm^{-3}. Our findings suggest new opportunities to confine light in this ubiquitous semiconductor and engineer the optical properties of nontraditional plasmonic materials.

Surface plasmons—collective charge oscillations at the interface between conductors and dielectrics—offer myriad new avenues to control the interaction of electromagnetic radiation with solid-state materials.[1] The noble metals, primarily Ag and Au, are frequently selected for this purpose because of their bulk plasma in the visible regime, ease of nanostructure synthesis, and stability under ambient conditions. Although control of nanoscale geometry provides a powerful means to modulate optical response, integration of metals into active devices[2] is complicated by fixed carrier concentrations and inadequate interface control.[3]

Semiconductors have emerged as an alternative, potentially more flexible class of plasmonic materials. Importantly, the carrier density of semiconductors, and thus surface plasmon frequency, can be modulated via chemical doping and/or electrostatic gating. This capability is a significant departure from the fixed carrier densities of metals and greatly expands the accessible design space.[2b,3b,4] The integration of plasmonic and excitonic function into a single active device may also lead to fundamentally new phenomena.[3a,c] Visible and near-infrared localized surface plasmon resonances (LSPRs) have been recently achieved in colloidal dispersions of heavily doped nanoscale semiconductors, including Cu_2S, Cu_2Se, ITO, and ZnO nanocrystals, as well as WO_3 nanorods.[3c,5]

Silicon's ubiquity in modern semiconductor device fabrication makes it an ideal system in which to manipulate surface plasmons. Its extensive knowledge base, including well-established methodologies for pattern formation, dopant delivery, interfacial control, and device integration, offers key advantages relative to other semiconductor systems.[2a,3b] The mid-infrared optical properties of heavily doped Si were originally reported over 50 years ago,[6] and recent studies further refine these results, showing that surface plasmon polaritons can be engineered in this system.[7] Subwavelength confinement of terahertz waves is also possible via excitation of LSPRs in Si microstructures;[8] however, the long wavelength of these modes limits their immediate utility.

Here, we identify mid-IR-tunable absorption modes resulting from phosphorus-doped Si nanowires synthesized via the vapor-liquid-solid (VLS) technique and assign these spectral features to longitudinal LSPRs. The optical response observed here, which requires large carrier densities, is distinct from that of nominally undoped Si nanowires in the visible regime.[9] VLS growth provides a straightforward way to achieve the necessary doping concentrations and simultaneously dictate nanowire geometry.[10] Our *in situ* absorption measurements offer direct access to nanowire LSPR frequency and bandwidth without the need for intermediate models or analyses. The clear observation of angle- and shape-dependent absorption features, which are strongly indicative of LSPRs, underscores the importance of controlling nanowire diameter, length, areal density, and epitaxial alignment. In addition, the *in situ* experiments performed here circumvent changes to LSPR frequency that would result from surface oxidation upon exposure to ambient.

Details of our *in situ* IR spectroscopy setup (Figure S1), nanowire growth protocols, and spectral acquisition procedures are provided in the Supporting Information. Briefly, a double-side polished Si(111) substrate is cleaned by high-temperature annealing *in situ*. A thin Au catalyst film is deposited via thermal evaporation upon cooling to room temperature. VLS growth proceeds via a two-step process that includes an initial incubation step followed by nanowire elongation. Si_2H_6 delivers Si atoms to the growing nanowire, and doping, when desired, is accomplished with PCl_3. Angle-dependent *in situ* absorption measurements are subsequently collected at room temperature in a transmission geometry for undoped and phosphorus-doped Si nanowires of different lengths.

Figure 1 displays scanning electron microscopy images of Si nanowire arrays grown on a Si(111) substrate with and without PCl_3 during the elongation step. The nanowires synthesized both with and without PCl_3 are epitaxially oriented and exhibit similar diameters and areal densities, as shown in Table 1 (Figure S2). Transmission electron microscopy reveals that all nanowires, doped or not, are single crystalline and ⟨111⟩ oriented (Figure S3). Nanowires exposed to PCl_3 during the

Received: August 1, 2012
Published: September 17, 2012

dx.doi.org/10.1021/ja3075902 | J. Am. Chem. Soc. 2012, 134, 16155−16158

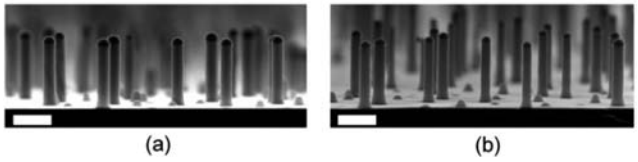

Figure 1. Cross-sectional SEM images of (a) undoped and (b) phosphorus-doped Si nanowire arrays. Scale bars, 400 nm.

Table 1. Dimensions and Array Areal Densities of Undoped and Phosphorus-Doped Si Nanowires

nanowire	length (nm)	diameter (nm)	density (nanowires-μm^{-2})
undoped	315 (±20)	70 (±10)	2.3 (±0.3)
doped	315 (±6)	64 (±10)	2.1 (±0.2)

elongation step exhibit a significantly accelerated etch rate in buffered hydrofluoric acid (Figure S4), which confirms the presence of phosphorus atoms.[11]

Despite the structural similarities between undoped and phosphorus-doped Si nanowire arrays, we observe a dramatic difference in their mid-IR optical response. Figure 2 compares

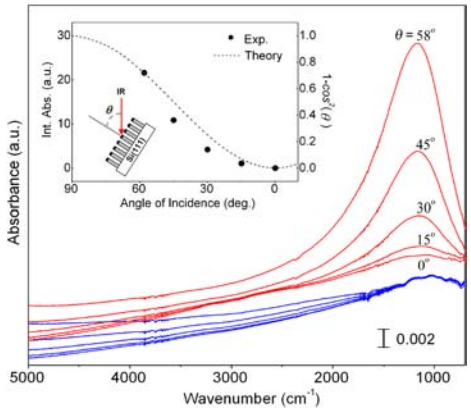

Figure 2. Absorption spectra for Si nanowires (L = 315 nm) as a function of angle of incidence, θ. Undoped and phosphorus-doped nanowires are shown in blue and red, respectively. Inset: Integrated peak intensity at each θ with respect to the minimum peak intensity (i.e., at $\theta = 0°$) for the phosphorus-doped nanowires plotted with the function $1 - \cos^2 \theta$ for comparison.

the absorption spectra for the two situations as a function of angle of incidence, θ. While the undoped nanowires exhibit nearly featureless spectra between 700 and 5000 cm^{-1}, an intense absorption peak centered at 1100 cm^{-1} appears for the phosphorus-doped nanowires. This angle-dependent mode is strongest at $\theta = 58°$ and decreases monotonically as θ approaches 0°. The peak maximum (ω_{max}) and full width at half-maximum (ω_{fwhm}) are largely invariant with angle of incidence (Figure S5). This absorption feature is not limited to nanowires with the dimensions shown in Figure 1. For example, phosphorus-doped nanowires with a length of 135 nm and the same diameter also display an intense and angle-dependent absorption band with a maximum at 1617 cm^{-1} (Figures S6 and S7). The observed peaks are moderately stable, shifting less than 100 cm^{-1} upon sample annealing to 650 °C or exposure to ambient laboratory air for 2 months.

The above results coupled with the following considerations indicate that the observed absorption bands result from the presence of phosphorus atoms in the Si nanowires themselves. Foremost, the clear difference between undoped and doped nanowires allows us to discount Mie resonances as the source of these modes.[9a] The Au catalyst at the tip of each nanowire can also be excluded via the same reasoning. Furthermore, similar modes are not seen following the exposure of Si_2H_6 and PCl_3 to a clean Si(111) substrate at relevant temperatures and pressures in the absence of a Au catalyst (Figure S8). Thus, conformal deposition of Si and phosphorus on the substrate or phosphorus diffusion into the substrate is not responsible for the absorption features in question. Spectral contributions from the substrate and/or nanowire phonon modes can also be excluded, as they are strongest at lower energies (500−1000 cm^{-1}) and are more narrow than the broad, intense peak observed here.[12]

We assign this prominent absorption band to a longitudinal LSPR that arises from heavy phosphorus-doping in the Si nanowires. The plot of phosphorus-doped nanowire integrated peak intensity at each angle of incidence, θ, with respect to the minimum peak intensity (i.e., $\theta = 0°$) in the inset of Figure 2 indicates that the dipole is oriented along the nanowire axis (i.e., perpendicular to the substrate), as would be expected for longitudinal LSPRs. The same $1 - \cos^2 \theta$ functional dependence is a common feature of LSPRs supported in metallic nanorods.[13] We note that free carrier absorption, which is a well-known behavior of heavily doped semiconductors and manifests as a continuously sloping baseline with a λ^2 dependence in the mid-IR,[6a] looks quite different from the clearly peaked feature seen here. As opposed to the current situation (Figure 2), free carrier absorption is not a strong function of substrate angle.

A systematic examination of absorption peak position as a function of phosphorus-doped nanowire length also supports the longitudinal LSPR assignment. Figure 3a shows representative phosphorus-doped Si nanowires with lengths ranging from 135 to 1160 nm. Nanowire diameters and array areal densities are largely constant since the same incubation step is used for all lengths (Figures S9 and S10). As displayed in the normalized spectra of Figure 3b and expected due to shape-dependent depolarization,[14] the LSPR mode red-shifts from 1632 to 741 cm^{-1} as the nanowires increase in length from 135 to 1160 nm. The fwhm values fluctuate between 770 and 1080 cm^{-1} (Table S1). Analysis of the spectra prior to normalization reveals that peak intensity is linearly proportional to nanowire length (Figure S11) as a result of the increasing polarizability volume.[14] We initially assign the weak mode near 2620 cm^{-1}, which becomes increasingly visible for longer nanowires, to the transverse LSPR (Figure S12).

Figure 3c plots the longitudinal LSPR absorption frequency as a function of nanowire length and compares these values against those determined from basic scattering theory.[1] The theoretical curves, determined via Mie−Gans theory assuming a Drude model for the free carriers and the physical properties of bulk Si (Supporting Information), predict the LSPR frequency for a range of doping concentrations. A comparison of experiment and theory reveals that our nanowires exhibit free carrier densities on the order of 10^{19}−10^{20} cm^{-3}. In addition, it appears that the phosphorus dopant concentration varies as a function of nanowire length. We attribute this behavior to unwanted radial deposition (Figure 3a), especially for longer nanowires (L > 400 nm), which modifies LSPR frequency by enhancing the dopant density near the surface and/or modifying the nanowire geometry. Both effects are frequently observed for VLS-grown semiconductor nanowires,[10d] and

dx.doi.org/10.1021/ja3075902 | J. Am. Chem. Soc. 2012, 134, 16155−16158

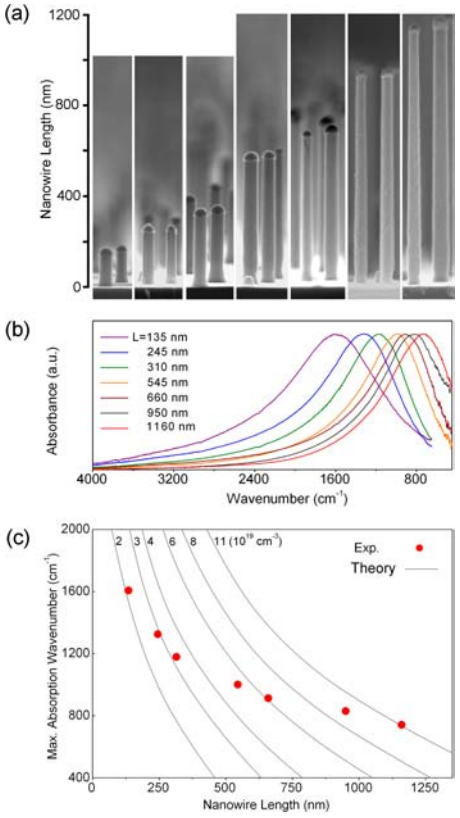

Figure 3. (a) SEM images of representative phosphorus-doped nanowires with an average diameter of 67 nm and lengths from 135 to 1160 nm. (b) Normalized IR absorption spectra at $\theta = 58°$ for the different length nanowires shown in (a). (c) Experimental absorption peak position from (b) as a function of nanowire length (red circles) plotted with a theoretical prediction of LSPR frequency (gray curves) determined via Mie–Gans theory, assuming a Drude model for the free carriers and the physical properties of bulk Si.

efforts are currently underway in our laboratory to improve doping uniformity and control sidewall taper. It is also important to note that Mie–Gans theory assumes uniform carrier density and symmetric structures, which limits its ability to robustly predict LSPR frequency for either of these situations. However, the estimated doping concentration of the shorter nanowires ($L < 400$ nm), where radial deposition is minimized (Figure 3a), is worthy of further discussion. Figure 3c indicates that these nanowires exhibit free carrier densities between 2×10^{19} and 4×10^{19} cm^{-3}. Assuming that all phosphorus atoms are electrically active, these dopant densities are comparable with those previously reported for doped Si and Ge nanowires[10d] and near the solid solubility of P in bulk Si at 500–550 °C (1.7×10^{19}–3.8×10^{19} cm^{-3}).[15]

The quality factor, Q, defined as the resonant frequency divided by the bandwidth, is an important indicator of loss.[16] We find a maximum $Q = 1.5$ for Si nanowires with $L < 400$ nm (Table S1). This value compares favorably with prior reports of mid-IR longitudinal LSPRs in micrometer-long Au nanorods.[17] We attribute some of the difference between the quality factors reported here for Si (Q = 1.2–1.5) and those of mid-IR resonant Au nanorods (Q = 2–3) to inhomogenous broadening in our ensemble measurements as a result of the inherent diameter distribution as well as the small but non-negligible coupling (*vide infra*) in our Si nanowire arrays. While we expect that a narrower distribution of nanowire diameters and spacings, achieved via lithographically defined catalyst arrays, will further improve the quality factor, additional work is required to more fully elucidate the connection between Si nanowire structure (morphology, sidewall faceting, dopant profile, etc.), growth chemistry, and LSPR damping.

It is well known that modulation of metallic nanoparticle optical response is possible via near-field dipolar and far-field radiative coupling.[18] Thus, it is important to preliminarily assess the extent of interaction between neighboring Si nanowires in the arrays studied here. Our results display a 300 cm^{-1} blue-shift of the longitudinal LSPR as the nanowire density increases from 2.1 to 11.1 nanowires-μm^{-2} (Figure S13). On the other hand, a reduction of nanowire density (i.e., <2.1 nanowires-μm^{-2}) generates a much smaller red-shift. These data confirm that the spectra shown in Figures 2 and 3 result largely from isolated LSPRs. The ability to control nanowire spacing via pregrowth catalyst patterning is a benefit of the bottom-up VLS technique and enables the direct manipulation of plasmon coupling in this system.

While the mid-IR Si nanowire LSPRs reported here (from 700 to 1600 cm^{-1}) are well suited for use in ultrasensitive chemical and biological detection,[19] more broadly tunable resonant frequencies would generate additional possibilities for manipulating optoelectronic and photonic function. For example, near-IR excitation may improve capture of long-wavelength photons in photovoltaic devices via two- or more-photon absorption processes.[20] Increasing the doping concentration and reducing the aspect ratio are the most immediate approaches to expand the spectral window for Si nanowire LSPRs. Mie–Gans theory indicates that uniformly doped Si nanowires with diameter and length of 70 and 135 nm, respectively, will require doping concentrations exceeding 3×10^{20} cm^{-3} to achieve LSPRs above 5000 cm^{-1}. While this P atom concentration is thermodynamically achievable at 750 °C,[15] the kinetically limited nature of VLS growth from hydride precursors[10a,21] and/or the strain relaxation inherent at the nanoscale[22] may enable highly metastable doping concentrations at lower temperatures. Furthermore, VLS growth offers sophisticated methods to control nanoscale structure and thus properties. For example, compositional and/or doping heterostructures are possible by modulating the delivery of precursors.[10a,c,d] Careful control of nanowire growth chemistry also provides new options for engineering morphology (orientation, faceting, etc.).[23]

In conclusion, we assign angle- and shape-dependent absorption modes, observed in the mid-IR for phosphorus-doped Si nanowires synthesized via the VLS technique, to longitudinal LSPRs. The extracted quality factors compare favorably to those of Au nanorods in this spectral regime. Analogous optical responses are also expected for any semiconductor nanowire system (III–V, etc.) where structure and doping can be similarly controlled. When combined with Si's extensive processing and device design knowledge base, our findings open the door to a range of new opportunities for this ubiquitous semiconductor.

■ ASSOCIATED CONTENT

Supporting Information

Nanowire growth protocols, spectroscopic methods, theoretical calculations, and additional figures, as referenced in the main text. This material is available free of charge via the Internet at http://pubs.acs.org.

dx.doi.org/10.1021/ja3075902 | J. Am. Chem. Soc. 2012, 134, 16155–16158

AUTHOR INFORMATION

Corresponding Author
michael.filler@chbe.gatech.edu

Notes
The authors declare no competing financial interest.

ACKNOWLEDGMENTS

The authors gratefully acknowledge financial support from the National Science Council of Taiwan (L.C.), the Camille and Henry Dreyfus Postdoctoral Program in Environmental Chemistry (L.C.), and the National Science Foundation (N.S., S.V.S.). TEM work was accomplished through ORNL's Shared Research Equipment (ShaRE) User Program, which is sponsored by the U.S. DOE Office of Basic Energy Sciences, with the assistance of M. Chi and J. Y. Howe. Discussions with V. E. Ferry were insightful and appreciated.

REFERENCES

(1) (a) Kreibig, U.; Vollmer, M. *Optical properties of metal clusters*; Springer: Berlin, 1995. (b) Maier, S. A. *Plasmonics: Fundamentals and Applications*; Springer: Berlin, 2007.
(2) (a) Walters, R. J.; van Loon, R. V. A.; Brunets, I.; Schmitz, J.; Polman, A. *Nat. Mater.* **2010**, *9*, 21. (b) Soref, R. *Nat. Photon.* **2010**, *4*, 495.
(3) (a) Zhang, J.; Tang, Y.; Lee, K.; Ouyang, M. *Nature* **2010**, *466*, 91. (b) Li, D.; Ning, C. Z. *Opt. Exp.* **2011**, *19*, 14594. (c) Luther, J.; Jain, P.; Ewers, T.; Alivisatos, P. *Nat. Mater.* **2011**, *10*, 361.
(4) (a) West, P. R.; Ishii, S.; Naik, G. V.; Emani, N. K.; Shalaev, V. M.; Boltasseva, A. *Laser Photon. Rev.* **2010**, *4*, 795. (b) Naik, G. V.; Liu, J.; Kildishev, A. V.; Shalaev, V. M.; Boltasseva, A. *Proc. Natl. Acad. Sci. U.S.A.* **2012**, *109*, 8834.
(5) (a) Zhao, Y.; Pan, H.; Lou, Y.; Qiu, X.; Zhu, J.; Burda, C. *J. Am. Chem. Soc.* **2009**, *131*, 4253. (b) Kanehara, M.; Koike, H.; Yoshinaga, T.; Teranishi, T. *J. Am. Chem. Soc.* **2009**, *131*, 17736. (c) Dorfs, D.; Härtling, T.; Miszta, K.; Bigall, N. C.; Kim, M. R.; Genovese, A.; Falqui, A.; Povia, M.; Manna, L. *J. Am. Chem. Soc.* **2011**, *133*, 11175. (d) Buonsanti, R.; Llordes, A.; Aloni, S.; Helms, B. A.; Milliron, D. J. *Nano Lett.* **2011**, *11*, 4706. (e) Scotognella, F.; Della Valle, G.; Srimath Kandada, A. R.; Dorfs, D.; Zavelani-Rossi, M.; Conforti, M.; Miszta, K.; Comin, A.; Korobchevskaya, K.; Lanzani, G.; Manna, L.; Tassone, F. *Nano Lett.* **2011**, *11*, 4711. (f) Hsu, S.-W.; On, K.; Tao, A. R. *J. Am. Chem. Soc.* **2011**, *133*, 19072. (g) Manthiram, K.; Alivisatos, A. P. *J. Am. Chem. Soc.* **2012**, *134*, 3995.
(6) (a) Spitzer, W.; Fan, H. Y. *Phys. Rev.* **1957**, *108*, 268. (b) Balkanski, M.; Aziza, A.; Amzallag, E. *Phys. Status Solidi B* **1969**, *31*, 323. (c) Allen, S. J., Jr.; Tsui, D. C.; Logan, R. A. *Phys. Rev. Lett.* **1977**, *38*, 980.
(7) (a) Chen, Y. B.; Zhang, Z. M. *J. Phys. D: Appl. Phys.* **2008**, *41*, 095406. (b) Shahzad, M.; Medhi, G.; Peale, R. E.; Buchwald, W. R.; Cleary, J. W.; Soref, R.; Boreman, G. D.; Edwards, O. *J. Appl. Phys.* **2011**, *110*, 123105. (c) Ginn, J. C.; Jarecki, J.; Robert, L.; Shaner, E. A.; Davids, P. S. *J. Appl. Phys.* **2011**, *110*, 043110.
(8) Berrier, A.; Ulbricht, R.; Bonn, M.; Rivas, J. G. *Opt. Exp.* **2010**, *18*, 23226.
(9) (a) Cao, L.; Fan, P.; Barnard, E. S.; Brown, A. M.; Brongersma, M. L. *Nano Lett.* **2010**, *10*, 2649. (b) Seo, K.; Wober, M.; Steinvurzel, P.; Schonbrun, E.; Dan, Y.; Ellenbogen, T.; Crozier, K. B. *Nano Lett.* **2011**, *11*, 1851.
(10) (a) Lauhon, L. J.; Gudiksen, M. S.; Lieber, C. M. *Philos. Trans. R. Soc. A* **2004**, *362*, 1247. (b) Schmidt, V.; Wittemann, J. V.; Gosele, U. *Chem. Rev.* **2010**, *110*, 361. (c) Frances, M. R. *Rep. Prog. Phys.* **2010**, *73*, 114501. (d) Wallentin, J.; Borgstrom, M. T. *J. Mater. Res.* **2011**, *26*, 2142.
(11) Williams, K. R.; Muller, R. S. *J. Microelectromech. Sci.* **1996**, *5*, 256.
(12) (a) Johnson, F. A. *Proc. Phys. Soc.* **1959**, *73*, 256. (b) Stierwalt, D. L.; Potter, R. F. *J. Phys. Chem. Solids* **1962**, *23*, 99.
(13) Pérez-Juste, J.; Rodríguez-González, B.; Mulvaney, P.; Liz-Marzán, L. M. *Adv. Funct. Mater.* **2005**, *15*, 1065.
(14) (a) Link, S.; Mohamed, M. B.; El-Sayed, M. A. *J. Phys. Chem. B* **1999**, *103*, 3073. (b) Hutter, E.; Fendler, J. H. *Adv. Mater.* **2004**, *16*, 1685. (c) Myroshnychenko, V.; Rodriguez-Fernandez, J.; Pastoriza-Santos, I.; Funston, A. M.; Novo, C.; Mulvaney, P.; Liz-Marzan, L. M.; Garcia de Abajo, F. J. *Chem. Soc. Rev.* **2008**, *37*, 1792.
(15) (a) Ostoja, P.; Nobili, D.; Armigliato, A.; Angelucci, R. *J. Electrochem. Soc.* **1976**, *123*, 124. (b) Olesinski, R.; Kanani, N.; Abbaschian, G. *J. Phase Equilib.* **1985**, *6*, 130.
(16) Sonnichsen, C.; Franzl, T.; Wilk, T.; von Plessen, G.; Feldmann, J.; Wilson, O.; Mulvaney, P. *Phys. Rev. Lett.* **2002**, *88*, 077402.
(17) (a) Neubrech, F.; Weber, D.; Lovrincic, R.; Pucci, A.; Lopes, M.; Toury, T.; de La Chapelle, M. L. *Appl. Phys. Lett.* **2008**, *93*, 163105. (b) Weber, D.; Albella, P.; Alonso-González, P.; Neubrech, F.; Gui, H.; Nagao, T.; Hillenbrand, R.; Aizpurua, J.; Pucci, A. *Opt. Exp.* **2011**, *19*, 15047.
(18) (a) Rechberger, W.; Hohenau, A.; Leitner, A.; Krenn, J. R.; Lamprecht, B.; Aussenegg, F. R. *Opt. Commun.* **2003**, *220*, 137. (b) Haynes, C. L.; McFarland, A. D.; Zhao, L.; Van Duyne, R. P.; Schatz, G. C.; Gunnarsson, L.; Prikulis, J.; Kasemo, B.; Käll, M. *J. Phys. Chem. B* **2003**, *107*, 7337. (c) Jain, P. K.; Eustis, S.; El-Sayed, M. A. *J. Phys. Chem. B* **2006**, *110*, 18243.
(19) Aroca, R. F.; Ross, D. J.; Domingo, C. *Appl. Spectrosc.* **2004**, *58*, 324A.
(20) Atwater, H. A.; Polman, A. *Nat. Mater.* **2010**, *9*, 205.
(21) Kodambaka, S.; Tersoff, J.; Reuter, M. C.; Ross, F. M. *Phys. Rev. Lett.* **2006**, *96*, 096105.
(22) Chan, C. K.; Peng, H.; Liu, G.; McIlwrath, K.; Zhang, X. F.; Huggins, R. A.; Cui, Y. *Nat. Nanotechnol.* **2008**, *3*, 31.
(23) (a) Tian, B.; Xie, P.; Kempa, T. J.; Bell, D. C.; Lieber, C. M. *Nat. Nanotechnol.* **2009**, *4*, 824. (b) Shin, N.; Filler, M. A. *Nano Lett.* **2012**, *12*, 2865.